Technical Note

Validation Tests for Discrete Element Codes Using Single-Contact Systems

Changsheng Li[1]; Hongwei Yin[2]; Dong Jia[3]; Jiaxing Zhang[4]; Wei Wang[5]; and Shijin Xu[6]

Abstract: In recent years, the discrete element method (DEM) has become widely used to solve a number of geological and geophysical problems. The basic idea of this method is to consider rock-soil bodies, in their discontinuous nature, as a set of discrete elements. It is generally recognized that this type of complex model must be validated through comparison with experimental results. Many researchers have addressed this in earlier publications. However, one important aspect has been given little attention, namely, testing the code to ensure that the computer program executes the model specification correctly. This paper describes in detail a DEM program for cohesionless particle vibration and shows four simple simulations used to verify the code. The results of these simulations are compared with PFC (Particle Flow Code 2D) and analytical solutions that are mathematically correct, showing that they have a good consistency. It is concluded that mathematical tests in artificial situations can uncover bugs in programs that appear to be running correctly, even if the programs simulate real experiments reasonably well. The simulation of relative error between numerical solutions and analytical solutions increases as artificial viscosity is introduced. These tests are published with the aim of helping others validate their programs (such as PFC) in similar applications. **DOI: 10.1061/(ASCE)GM.1943-5622.0001133.** © *2018 American Society of Civil Engineers.*

Author keywords: DEM; Lattice solid model; Numerical solution; Analytical solution; PFC.

Introduction

Granular media are one of the most common material types existing on earth: they are widely distributed, and furthermore, they have complex mechanical characteristics. Cundall and Strack (Cundall and Strack 1979) presented a discrete element method (DEM) capable of describing the mechanical behavior of assemblies of granular media. Its basic idea is to consider the discontinuous nature of granular materials as a set of discrete elements. During the initial period, its research object mainly focused on discontinuous medium such as rock and soil. Through decades of exploration and development, DEM has come to have a wide range of applications in many engineering and scientific fields. Without the assumptions of continuity, DEM permits large relative motion inside the model and simulates its evolution dynamically (Morgan 2015; Yin et al. 2009). In recent decades, the DEM has been applied to the study of geological and geophysical problems (Botter et al. 2016; Burbidge and Braun 2002; Finch et al. 2003; Hardy and Finch 2006; Morgan 2015; Saltzer and Pollard 1992; Schöpfer et al. 2016; Yin et al. 2009; Zhang et al. 2013). The DEM described here is a variant of the lattice solid model (LSM), which has been used to simulate the dynamical process associated with earthquakes (Mora and Place 1993; Mora and Place 1994; Mora and Place 1998; Place and Mora 1999; Place and Mora 2001a; Matsu'ura et al. 2002). Generally, the LSM does not include particle resistance to rolling in this model (Hardy et al. 2009; Iwashita and Oda 2000). However, it is able to address a number of geological and geophysical problems (Hardy et al. 2009; Liu et al. 2015; Liu et al. 2013; Liu et al. 2017; Mora et al. 2015; Morgan 1999; Morgan 2015; Morgan and Boettcher 1999; Yin et al. 2009; Zhang et al. 2013).

It has generally been recognized that DEM must be validated through a comparison with experimental results. Many researchers have addressed this in earlier publications (Antonellini and Pollard 1995; Damjanac and Cundall 2016; Kazerani and Zhao 2010; Liu et al. 2015; Liu et al. 2013; Place and Mora 2001b; Shi et al. 2016). However, one important aspect is often given little attention, and that is testing the code to ensure that the computer program executes the model specification correctly. Even if a program appears to simulate real experiments reasonably well, there may nevertheless be many bugs in it. Chen et al. (2007) investigated a series of simple, one and two-particle contact problems with two DEM solutions [PFC2D (Itasca 2004) and YADE (Smilauer et al. 2017)], which yield identical solutions to such problems, provided the solution process is properly manipulated. Asmar et al. (2002) described in detail a DEM program for cohesive particle vibration and showed some simple simulations that had helped to verify the code. They concluded that these mathematical tests of artificial situations could uncover bugs in programs. Such tests constituted a benchmark that could be used by others to test their own programs. They were useful, even if no analytical solutions were given. The mechanics of an aggregate of particles in multiple contact is complicated and few or no analytical solutions are available. Balevičius et al. (2004)

[1]Ph.D. Candidate, School of Earth Sciences and Engineering, Nanjing Univ., 163 Xianlin Road, Nanjing 210023, China. Email: lichangsheng@samil.nju.edu.cn

[2]Professor, School of Earth Sciences and Engineering, Nanjing Univ., 163 Xianlin Road, Nanjing 210023, China (corresponding author). Email: hwyin@nju.edu.cn

[3]Professor, School of Earth Sciences and Engineering, Nanjing Univ., 163 Xianlin Road, Nanjing 210023, China. Email: djia@nju.edu.cn

[4]Postgraduate Student, School of Earth Sciences and Engineering, Nanjing Univ., 163 Xianlin Road, Nanjing 210023, China. Email: gaci2318@163.com

[5]Ph.D. Candidate, School of Earth Sciences and Engineering, Nanjing Univ., 163 Xianlin Road, Nanjing 210023, China. Email: wangwei09@outlook.com

[6]Professor, School of Earth Sciences and Engineering, Nanjing Univ., 163 Xianlin Road, Nanjing 210023, China. Email: xusj@nju.edu.cn

Note. This manuscript was submitted on April 14, 2017; approved on November 3, 2017; published online on March 29, 2018. Discussion period open until August 29, 2018; separate discussions must be submitted for individual papers. This technical note is part of the ***International Journal of Geomechanics***, © ASCE, ISSN 1532-3641.

checked the unidirectional contact motion test of a single particle and compared the results with the analytical solutions. Only normal contact force was considered, and shear force was set to zero. This is because contact theory is complex and no analytical solutions would exist if shear contact force was introduced. However, the mathematical analytical solutions involving normal contact force and shear contact force can be obtained on single-contact particle systems by simplifying contact mechanics models such as LSM.

This paper describes a general purpose two-dimensional DEM program (as implemented in Virtual Sandbox, or VBOX) and presents four single contact particle systems used to validate the code. The "DEM" section describes the DEM technique and the modeling method in detail. The "Validation Tests" section shows four tests that were used as part of the code validation. The results calculated by VBOX are compared with PFC2D (Itasca 2004) and the mathematical analytical solutions; they are found to have good consistency.

DEM

A geological body is simplified into an assemblage of circular elements that can move under the action of the forces generated through paired interactions with springs. Although we assumed that the geological medium under consideration was cohesionless, and thus all springs were not tensile (Hardy and Finch 2006), the models were able to capture complex features of fault evolution and produce realistic fault geometries and strain fields (Botter et al. 2014; Hardy et al. 2009).

As shown in Fig. 1, let us consider two particles with the centers $o(x_o, y_o)$, $a(x_a, y_a)$ and radii are r_o, r_a that enter into contact. The unit normal vector, $\overrightarrow{n}$, is defined as (n_1, n_2), and the unit tangent vector, $\overrightarrow{t}$, is defined as $(-n_2, n_1)$ (Itasca 2004). n_1, n_2 are given by

$$n_1 = \frac{x_a - x_o}{|\overrightarrow{oa}|} \tag{1}$$

$$n_2 = \frac{y_a - y_o}{|\overrightarrow{oa}|} \tag{2}$$

where $|\overrightarrow{oa}|$ is the distance between the particles' centers,

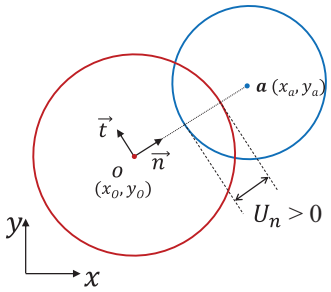

Fig. 1. Definition of the unit normal vector and unit tangent vector. If two particles overlap each other, a repulsive force will come into being.

$$|\overrightarrow{oa}| = \sqrt{(x_a{}^2 - x_o{}^2) - (y_a{}^2 - y_o{}^2)} \tag{3}$$

The normal contact force F_n between the particles is a repulsive force, which is given by

$$F_n = K_n U_n \tag{4}$$

where K_n is the normal stiffness at the contact and U_n is the normal relative displacement. We define that positive value of the normal contact force denotes compression. Then, $U_n = (r_o + r_a) - |\overrightarrow{oa}|$. When the two particles are in an equilibrium state, $U_n = 0$. If they overlap with each other (i.e., $U_n > 0$), a repulsive force will come into being. Because we assume that springs cannot take tension, there cannot be an attractive force between the particles.

In addition to the normal contact force, F_n, the shear contact force, F_s, was also considered (Hardy et al. 2009; Liu et al. 2013; Place and Mora 1999). The shear contact force was computed in an incremental fashion. When the contact was formed, the total shear contact force was initialized to zero. Each subsequent relative shear-displacement increment resulted in an increment of elastic shear force that was added to the current value (Itasca 2004). Because the shear contact force was calculated using an incremental form, a handy symbol was introduced for convenience, as shown in Fig. 2. For example, $F_s{}^{-}$ denotes the shear contact force of the previous step, $F_s{}^{\circ}$ is the shear contact force of the current step, and $v^{\ominus}$ is the mean velocity during the previous step. Therefore, the normal contact force of the current step calculated by Eq. (4) can be denoted as $F_n{}^{\circ}$, and all relevant symbols are the value of the current step when the normal contact force was described in the above context.

The shear contact force of the current step, $F_s{}^{\circ}$, is determined by

$$F_s{}^{\circ} = F_s{}^{-} - K_s \, v_s{}^{\ominus} \Delta t \tag{5}$$

where $F_s{}^{-}$ is the old shear force at the start of the time step, and K_s is the shear stiffness at the contact. We did not include particle resistance to rolling in this model (Hardy et al. 2009; Iwashita and Oda 2000), i.e., the particle spins were initially set to zero and fixed in the whole simulation, so the mean shear velocity during the previous step, $v_s{}^{\ominus}$, is given by

$$v_s{}^{\ominus} = \left(\overrightarrow{v_a{}^{\ominus}} - \overrightarrow{v_o{}^{\ominus}}\right) \cdot \overrightarrow{t^{\circ}} \tag{6}$$

where $\overrightarrow{v_a{}^{\ominus}}$ and $\overrightarrow{v_o{}^{\ominus}}$ are the velocities of particle a and o, respectively, during the previous step.

The magnitude of the shear contact force must be less than or equal to the maximum shear force, $F_{s_{max}}{}^{\circ}$ allowed by Coulomb friction,

$$F_{s_{max}}{}^{\circ} = \mu F_n{}^{\circ} \tag{7}$$

$$F_s{}^{\circ} = F_{s_{max}}{}^{\circ} (if \; F_s{}^{\circ} > F_{s_{max}}{}^{\circ}) \tag{8}$$

Therefore, the forces by which particle a finally acts on particle o are $\overrightarrow{F_{o,a}{}^{\circ}} = (F_n{}^{\circ}, F_s{}^{\circ})$.

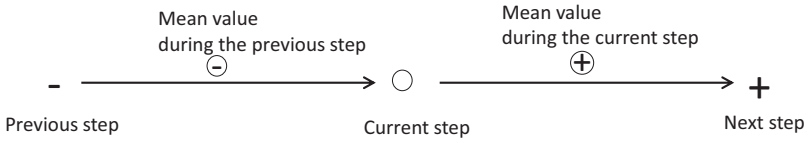

Fig. 2. Interpretation of a handy symbol.

In numerical simulations, a viscous damping term was added to avoid buildup of kinetic energy in the closed system (Finch et al. 2003; Mora and Place 1993; Mora and Place 1994; Matsu'ura et al. 2002). Additionally, gravitational forces acting on each element were calculated. Therefore, the resultant force on any particle is given by

$$\overrightarrow{F_o^{\circ}} = \sum \overrightarrow{F_{o,\alpha}^{\circ}} - \eta \overrightarrow{v_o^{\ominus}} + m_i \overrightarrow{g} \tag{9}$$

where η represents the artificial viscosity, $\overrightarrow{v_o}$ is the mean velocity of the particle o during the previous step, and m_i is its mass. $\overrightarrow{g}$ is gravitational acceleration. The number of contact with particle o is α. $\sum \overrightarrow{F_{o,\alpha}^{\circ}}$ denotes the sum of the force that every particle acts on particle o.

The motion of a single particle was determined by the resultant force. The numerical integration was based on leapfrog scheme. Integrating motion consisted of using current acceleration $\overrightarrow{a^{\circ}}$ on a particle to update its position from the current value $\overrightarrow{P^{\circ}}$ to its value at the next time step $\overrightarrow{P^{+}}$. Computation of acceleration, knowing the current resultant force $\overrightarrow{F^{\circ}}$ acting on a particle and its mass m, is simply

$$\overrightarrow{a^{\circ}} = \overrightarrow{F^{\circ}}/m \tag{10}$$

The positions of the next step $\overrightarrow{P^{+}}$ and the mean velocity $\overrightarrow{v^{\oplus}}$ of the particles during current step are calculated from

Table 1. Model Data

Quantity	Value
Density (ρ)	2.5000×10^3 kg·m^{-3}
Radii (r)	50.0000 m
Normal contact stiffness (K_n)	5.5000×10^9 N·m^{-1}
shear contact stiffness (K_s)	5.5000×10^9 N·m^{-1}
Friction coefficient (μ)	0.1000
Artificial viscosity (η)	3.0000×10^8 N·s·m^{-1}
Time step (Δt)	1.0000×10^{-3} s

$$\overrightarrow{v^{\oplus}} = \overrightarrow{v^{\ominus}} + \overrightarrow{a^{\circ}}\Delta t \tag{11}$$

$$\overrightarrow{P^{+}} = \overrightarrow{P^{\circ}} + \overrightarrow{v^{\oplus}}\Delta t \tag{12}$$

Validation Tests

The program VBOX is written in C to implement the algorithm described above. VBOX starts by reading all input variables from a file, performing the calculations at each time step. It stores the position, velocity, and force information for all particles. It can run on all Linux operating systems. This section shows four special tests. They are not exhaustive but are shown to help other researchers develop tests for their code. Table 1 shows the model data used for the validation tests. Gravitational acceleration is set to zero. The intended application of this program is to study problems on a geological scale, and thus the radii of the particles are set to 50 m.

The Normal Contact Force

To test for the particle–particle normal contact force implementation, a free particle with an initial velocity, $\overrightarrow{v_a} = (v_{ax}, v_{ay}) = (0.0000, -0.1000)$ m/s hits a stationary particle, as shown in Fig. 3. Notice that their horizontal motion is restricted. The analytical solutions are given in Eqs. (14)–(17) in the Appendix.

T1 is without viscosity, and Particle 2 moves downward at first with the given initial velocity $\overrightarrow{v_a}$. The repulsive force between Particle 1 and Particle 2 slows Particle 2 and changes its direction of motion when t approaches 0.1, as shown in Fig. 3. The initial conditions for Eq. (14) depend on Eq. (15), and the initial conditions for Eq. (16) depend on Eq. (17). All solutions for Eqs. (14)–(17) can be calculated. When Particle 2 returns to the origin, $y|_{t=t_{n1}} = 0$, t_{n1} can be solved using these conditions and then v_{n1} can be solved. Similar to T1, t_{n2} and v_{n2} in the T2 with viscosity can be solved by Eqs. (16) and (17).

Fig. 3 shows the motion curve of Particle 2 from VBOX, PFC (2D), and the analytical solution. Eqs. (14)–(17) in the Appendix

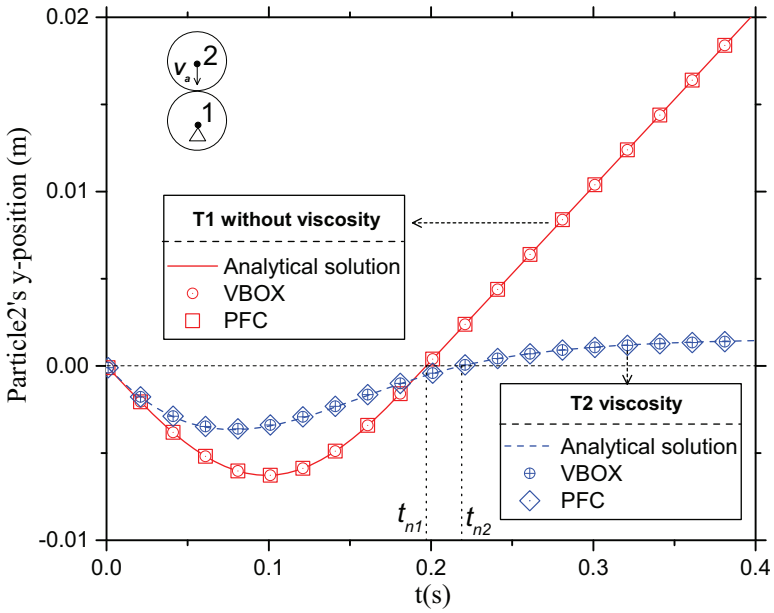

Fig. 3. Particle 2's motion curve of the VBOX, PFC, and analytical solutions. The x and y coordinates of Particle 1 are fixed, and an initial velocity is given to Particle 2. Note that the initial coordinates of Particle 2's center are the coordinate origin, i.e., (0,0). The analytical solution is obtained from Eqs. (14)–(17). The artificial viscosity of the T1 is zero. Analogously, the artificial viscosity of the T2 is 3.0000×10^8 N·s·m^{-1}.

are solved to construct the analytical curves in Fig. 3 by MATLAB. The MATLAB codes for the analytical solutions are provided in the Supplemental Data. Note that initial coordinates of Particle 2's center are those of the coordinate origin, i.e., (0,0). When viscosity is zero, the solid line is obtained from the analytical solution using Eqs. (14) and (15) and the circles and squares are the results calculated from numerical simulations by the VBOX and PFC (2D) (Itasca 2004), respectively. The relevant PFC codes are provided in the Supplemental Data. Analogously, when the artificial viscosity is 3.0000×10^8 N·s·m^{-1}, the dashed line is obtained from analytical solution using Eqs. (16) and (17), and the circles with plus signs and diamonds are the results calculated from numerical simulations by the VBOX and PFC, respectively. There is no movement in the x direction and no rotation. When artificial viscosity is introduced, the extent of motion of the particle is reduced. When it begins to move free ($t > t_{n2}$), its velocity decreases under the action of artificial viscosity and it becomes immobile in the end.

The relative error of T1 and T2 (the difference between the analytical solution and the simulation solution) is shown in Fig. 4, where Fig. 4(a) depicts the no viscosity case (i.e. T1) and Fig. 4(b) the case with viscosity (i.e., T2). The results of PFC are completely consistent with VBOX. The simulation relative error of VBOX and PFC both increases as the artificial viscosity is introduced.

Shear Contact Force

To test for the shear contact force implementation, a free Particle 4 with an initial velocity of $\overrightarrow{v_b} = (v_{bx}, v_{by}) = (0.0000,\ 1.0000)$ m/s was simulated with a static wall 3 overlap, as shown in Fig. 5. The

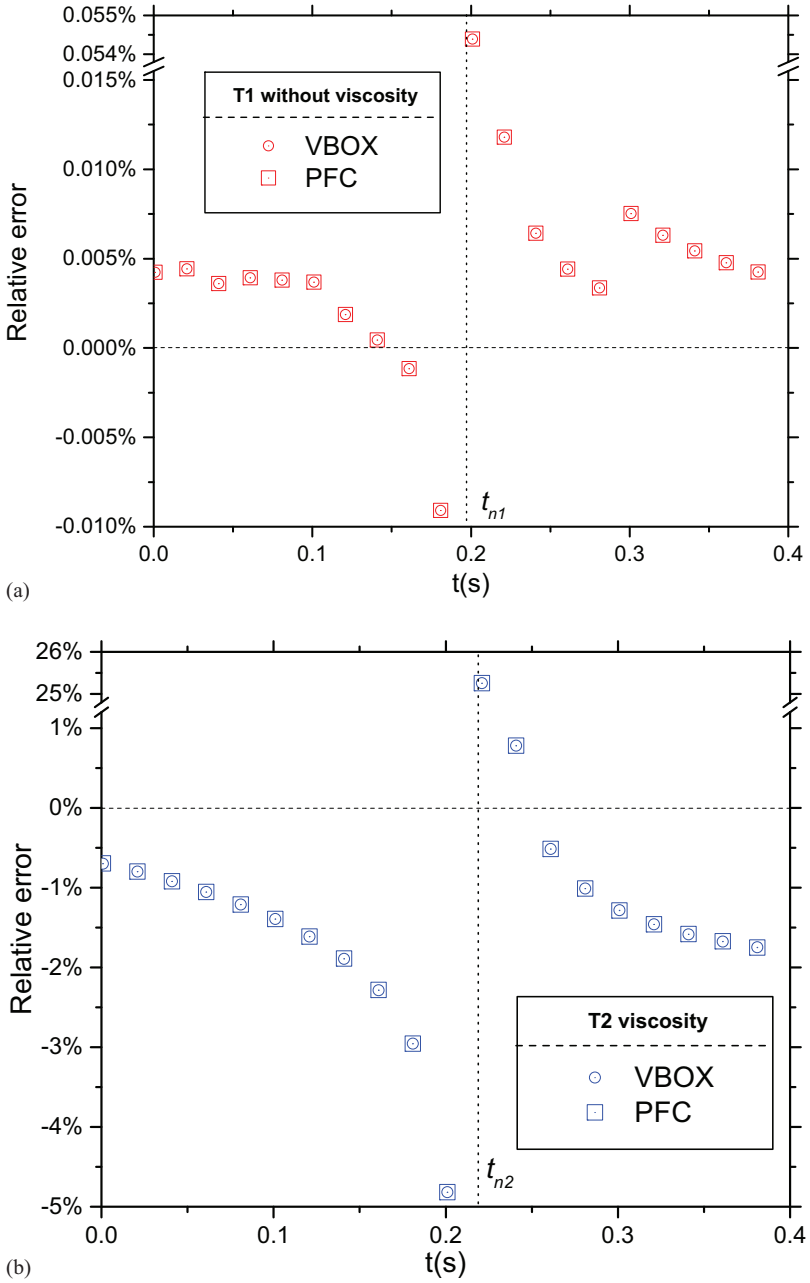

Fig. 4. Relative error of T1 and T2 (the difference between the analytical solutions and the simulation solutions): (a) T1 without viscosity; and (b) T2 with viscosity.

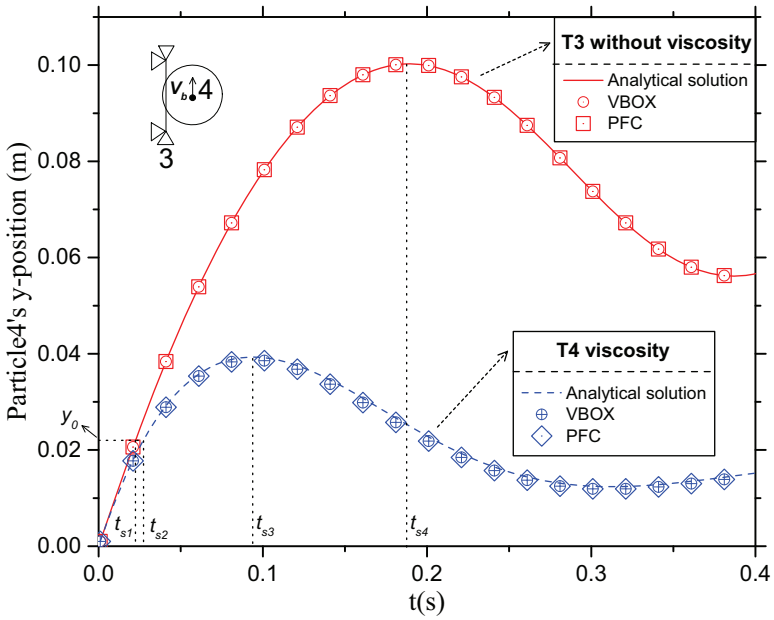

Fig. 5. Particle 4's motion curve for the VBOX, PFC and analytical solutions. The displacement of Wall 3 along the x and y directions is fixed, and an initial velocity is given to Particle 4. Note that the initial coordinates of Particle 4's center are the coordinate origin, i.e., (0,0). The analytical solution is obtained from Eqs. (18)–(23). The artificial viscosity of T3 is zero. Analogously, the artificial viscosity of the T4 is 3.0000×10^8 N·s·m^{-1}.

value of the overlap between Particle 2 and Wall 1, Δx, is equal in T3 and T4. In addition, their horizontal motion is restricted. The analytical solutions are given in Eqs. (18)–(23) in the Appendix.

The T3 is without viscosity. As Particle 2 moves along Wall 1, it goes through three stages. In the first stage, it moves under the action of the shear contact force calculated as the time integral of the tangential velocity of the contact using Eq. (5) during the time that the Coulomb friction $F_s < \mu F_n$ is satisfied. The critical sliding condition is $F_s = \mu F_n$, as $F_s = k_s y_1$ and $F_n = k_n \Delta x$, thus the critical tangential displacement $y_1 = \mu k_n \Delta x / k_s$. In the second stage, it enters into the sliding stage and the sliding friction force is constant, i.e., $F_s = \mu F_n$ and $a = F_s/m = \mu F_n/m$. When the velocity is reduced to zero with the action of the sliding friction force, the particle will change its direction of motion at t_{s4}. In the third stage, it returns to a stage similar to the first, but with an equilibrium position that adds up to b, which is the sliding distance for the second stage, i.e., $b = y_4 - y_1$.

T4 is identical to T3 but with a nonzero viscosity, η. The solution to Eq. (21) in the Appendix is

$$y(t) = v_{by}/\sqrt{k^2 - n^2} \cdot e^{-nt} \sin\left(\sqrt{k^2 - n^2}t\right) \tag{13}$$

Δx has been set to equality for T3 and T4, so the critical tangential displacement $y|_{t=t_{s2}} = y_2 = y_1 = \mu k_n \Delta x / k_s$. When we plug this into the transcendental Eq. (13), t_{s2} has no analytical solution. Let $\Delta x = v_{by}/\sqrt{k^2 - n^2} \cdot e^{-n\pi/\left(8\sqrt{k^2-n^2}\right)} \sin\left(\sqrt{k^2 - n^2} \cdot \pi / \left(8\sqrt{k^2 - n^2}\right)\right) \cdot k_s/(\mu k_n) \approx 0.2206$ m; then $y|_{t=t_{s2}} = y_2 = e^{-nt_{s2}} \cdot \sin\left(\sqrt{k^2 - n^2} \cdot t_{s2}\right)$. The exact t_{s2} can be obtained, i.e., $t_{s2} = \pi/\left(8\sqrt{k^2 - n^2}\right)$. As with T2, the sliding distance in the second stage, $d = y_3 - y_2$.

Fig. 5 shows Particle 4's motion curve for the VBOX, PFC, and analytical solutions. Eqs. (18)–(23) in the Appendix are solved to construct the analytical curves of Fig. 5 by MATLAB. Those MATLAB codes for analytical solutions are provided in the Supplemental Data. The displacement of Wall 3 along x and y direction is fixed, and an initial velocity is given to Particle 4. Note that initial coordinates of Particle 4's center are the coordinate origin, i.e., (0,0). A solid line is obtained from the analytical solution without viscosity using Eqs. (18)–(20) in the Appendix, and the circles and squares denote the results calculated from numerical simulations by VBOX and PFC, respectively. The relevant PFC codes are also provided in the Supplemental Data. Analogously, the dashed line is obtained from analytical solution with viscosity using Eqs. (21)–(23) in the Appendix, and the circles with plus signs and diamonds are the results calculated from numerical simulations by VBOX and PFC, respectively. There is no movement in the x direction and no rotation. When viscosity is introduced, the extent of motion of the particle is reduced, similar to T1 and T2. The results in Fig. 3 as calculated by VBOX are closer to the analytical solution than in Fig. 5; i.e., the accuracy is somewhat less than that recorded for the normal force measurement. Because the shear force is calculated as the time integral of the tangential velocity of the contact using Eq. (5), cumulative error will be caused and the normal contact force calculated using Eq. (4) has no cumulative error precision (Itasca 2004).

The relative error of the T3 and T4 is shown in Fig. 6, where Fig. 6(a) is for the no viscosity case (i.e., T3) and Fig. 6(b) is for the case with viscosity (i.e., T4). The results of PFC are completely consistent with VBOX, and the simulation relative error of VBOX and PFC both increases as the artificial viscosity is introduced. T3 and T4 are used to test the shear contact force of the single-contact systems. It requires relative velocity as input and returns the shear contact force as function of the accumulated deformation, as shown in Eq. (5), which will inevitably introduce an accumulation of error (Itasca 2004; Luding 2008); i.e., the magnitude of error is greater with greater time. Therefore, the error of the numerical simulation results with T3 and T4 will be greater than for T1 and T2. In other words, the numerical solutions (VBOX and PFC) of the normal contact force are more exact than the shear contact force.

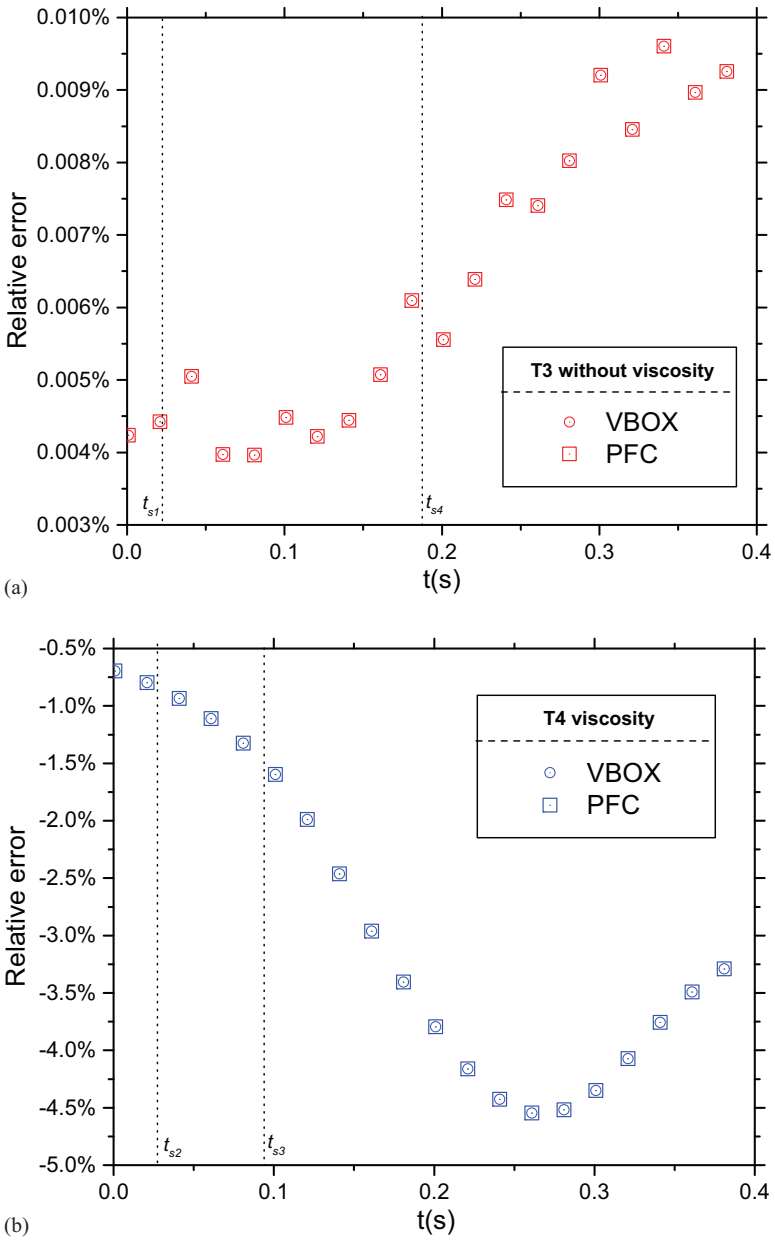

Fig. 6. Relative errors of T3 and T4 (the difference between the analytical solution and the simulation solution): (a) T3 without viscosity; and (b) T4 with viscosity.

Conclusion

VBOX, a 2D DEM program to simulate geological and geophysical problems using the C language, has been developed. Normal force, shear force, and viscosity were accounted for. Four tests to validate the code and their results were presented and compared with PFC and the analytical solutions to ensure that the computer program correctly executed the model specification. The simulated results have a good consistency with PFC and give analytical solutions that are mathematically correct. These mathematical tests of artificial situations can uncover bugs in programs that appear to be running correctly, even if they appear to simulate real experiments reasonably well. On the other hand, the results of PFC are completely consistent with VBOX. The simulated relative error between the numerical solutions (VBOX and PFC) and analytical solutions increases as the artificial viscosity is introduced. The tests constitute a benchmark that can be used by others to test their programs. These programs can be used for different scenarios with minor developments.

Appendix. Differential Equations

The differential equations for the tests of the normal contact force are listed as follows:

- T1:

$$\begin{cases} \ddot{y} + k^2 y = 0 \\ y|_{t=0} = 0 \quad \textit{Initial displacement} \\ \dot{y}|_{t=0} = v_{ay} \quad \textit{Initial velocity} \\ 0 \le t < t_{n1} \end{cases} \tag{14}$$

$$\begin{cases} \ddot{y} = 0 \\ y|_{t=t_{n1}} = 0 \quad \textit{Initial displacement} \\ \dot{y}|_{t=t_{n1}} = v_{n1} \quad \textit{Initial velocity} \\ t_{n1} \le t < 0.4 \end{cases} \tag{15}$$

- T2:

$$\begin{cases} \ddot{y} + 2n\dot{y} + k^2 y = 0 \\ y|_{t=0} = 0 \quad \textit{Initial displacement} \\ \dot{y}|_{t=0} = v_{ay} \quad \textit{Initial velocity} \\ 0 \le t < t_{n2} \end{cases} \tag{16}$$

$$\begin{cases} \ddot{y} + 2n\dot{y} = 0 \\ y|_{t=t_{n2}} = 0 \quad \textit{Initial displacement} \\ \dot{y}|_{t=t_{n2}} = v_{n2} \quad \textit{Initial velocity} \\ t_{n2} \le t < 0.4 \end{cases} \tag{17}$$

Note: n, k, v_{ay}, v_{n1}, v_{n2}, t_{n1}, and t_{n2} are given below. These differential equations are solved to construct the analytical curves of Fig. 3 by MATLAB. Those MATLAB codes for analytical solutions are provided in the Supplemental Data.

The differential equations for the tests of the shear contact force are listed as follows:

- T3:

$$\begin{cases} \ddot{y} + k^2 y = 0 \\ y|_{t=0} = 0 \quad \textit{Initial displacement} \\ \dot{y}|_{t=0} = v_{by} \quad \textit{Initial velocity} \\ 0 \le t < t_{s1} \end{cases} \tag{18}$$

$$\begin{cases} \ddot{y} + a = 0 \\ y|_{t=t_{s1}} = y_1 \quad \textit{Initial displacement} \\ \dot{y}|_{t=t_{s1}} = v_{s1} \quad \textit{Initial velocity} \\ t_{s1} \le t < t_{s4} \end{cases} \tag{19}$$

$$\begin{cases} \ddot{y} + k^2(y - b) = 0 \\ y|_{t=t_{s4}} = y_4 \quad \textit{Initial displacement} \\ \dot{y}|_{t=t_{s4}} = 0 \quad \textit{Initial velocity} \\ t_{s4} \le t < 0.4 \end{cases} \tag{20}$$

- T4:

$$\begin{cases} \ddot{y} + 2n\dot{y} + k^2 y = 0 \\ y|_{t=0} = 0 \quad \textit{Initial displacement} \\ \dot{y}|_{t=0} = v_{by} \quad \textit{Initial velocity} \\ 0 \le t < t_{s2} \end{cases} \tag{21}$$

$$\begin{cases} \ddot{y} + 2n\dot{y} + c = 0 \\ y|_{t=t_{s2}} = y_2 \quad \textit{Initial displacement} \\ \dot{y}|_{t=t_{s2}} = v_{s2} \quad \textit{Initial velocity} \\ t_{s2} \le t < t_{s3} \end{cases} \tag{22}$$

$$\begin{cases} \ddot{y} + 2n\dot{y} + k^2(y - d) = 0 \\ y|_{t=t_{s3}} = y_3 \quad \textit{Initial displacement} \\ \dot{y}|_{t=t_{s3}} = 0 \quad \textit{Initial velocity} \\ t_{s3} \le t < 0.4 \end{cases} \tag{23}$$

Note: n, k, y_1, y_2, y_3, y_4, v_{by}, v_{n1}, v_{n2}, t_{s1}, t_{s2}, t_{s3}, and t_{s4} are given below. These differential equations are solved to construct the analytical curves of Fig. 5 by MATLAB. Those MATLAB codes for analytical solutions are provided in the Supplemental Data.

The values in Eqs. (14)–(23) are given below.

$$m = 2\sqrt{3}\rho r^2 = 2.1651 \times 10^7 \ kg \ \text{(Place et al. 2002)} \tag{24}$$

$$n = \frac{\eta}{2m} \approx 6.9281 \ s^{-1} \tag{25}$$

$$k = \sqrt{\frac{k_n}{m}} = \sqrt{\frac{k_s}{m}} \approx 15.9383 \ s^{-1} \tag{26}$$

$$v_{ay} = -0.0100 \ m/s \tag{27}$$

- *T1*

$$t_{n1} = \frac{\pi}{k} \approx 0.1971 \ \text{s} \tag{28}$$

$$v_{n1} = v_{ay} = 0.1000 \ m/s \tag{29}$$

- *T2*

$$t_{n2} = \frac{\pi}{\sqrt{k^2 - n^2}} \approx 0.2189 \ s \tag{30}$$

$$v_{n2} = -v_{ay} e^{-n\pi/\sqrt{k^2 - n^2}} \approx 0.0220 \ m/s \tag{31}$$

$$v_{by} = 1.0000 \ m/s \tag{32}$$

$$\Delta x \approx 0.2206 \ m \tag{33}$$

- *T3*

$$y_1 = \frac{\mu k_n \Delta x}{k_s} \approx 0.0221 \ m \tag{34}$$

$$t_{s1} = \frac{1}{k} \sin^{-1}\left(\frac{y_1 k}{v_{by}}\right) \approx 0.0224 \ s \tag{35}$$

$$v_{s1} = v_{by} \cdot \cos(k t_{s1}) \approx 0.9367 \ m/s \tag{36}$$

$$a = \frac{\mu F_n}{m} \approx 5.6033 \ m/s^2 \tag{37}$$

$$t_{s4} = \frac{C_1}{a} \approx 0.1896 \ s \tag{38}$$

$$y_4 = y|_{t=t_{s4}} = \frac{-a{t_{s4}}^2}{2} + C_1 t_{s4} + C_2 \approx 0.1003 \ m \tag{39}$$

where

$$C_1 = v_{s1} + at_{s1} \approx 1.0625 \tag{40}$$

$$C_2 = y_1 + \frac{at_{s1}{}^2}{2} - C_1 t_{s1} \approx -0.0005 \tag{41}$$

$$b = y_4 - y_1 \approx 0.0782\ m \tag{42}$$

- *T4*

$$y_2 = y_1 \approx 0.0221\ m \tag{43}$$

$$t_{s2} = \frac{\pi}{8\sqrt{k^2 - n^2}} \approx 0.0274\ s \tag{44}$$

$$v_{s2} = \frac{v_{by}}{\sqrt{k^2 - n^2}} \cdot e^{-nt_{s2}} \cdot \left[\sqrt{k^2 - n^2}\cos\left(\sqrt{k^2 - n^2}t_{s2}\right) - n\sin\left(\sqrt{k^2 - n^2}t_{s2}\right)\right] \approx 0.6115\ m/s \tag{45}$$

$$t_{s3} = \frac{-ln\frac{-c}{4C_3n^2}}{2n} \approx 0.0938\ s \tag{46}$$

$$y_3 = C_4 + C_3 e^{-2nt_{s3}} - \frac{c}{2n} \cdot t_{s3} = 0.0393\ m \tag{47}$$

where

$$C_3 = \frac{v_{s2} + \frac{c}{2n}}{-2ne^{-2nt_{s2}}} \approx -0.1071 \tag{48}$$

$$C_4 = y_2 + \frac{c}{2n}t_{s2} - C_3 e^{-2nt_{s2}} \approx 0.1064 \tag{49}$$

$$c = \frac{\mu F_n}{m} = 5.6033\ m/s^2 \tag{50}$$

$$d = y_3 - y_2 \approx 0.0173\ m \tag{51}$$

Acknowledgments

The authors gratefully acknowledge the financial support provided by the National Natural Science Foundation of China (Grants 41272227, 41572187), National S&T Major Project of China (Grants 2016ZX05026-002-007, 2016ZX05003-001, 2016ZX005008-001-005), and the National Basic Research Program of China (973 Program Grant 2012CB214703). Changsheng Li is supported by the Program B for Outstanding Ph.D. Candidate of Nanjing University. The authors thank Prof. Julia Morgan for generously sharing her discrete element code RICEBAL (v. 5.4, modified from Peter Cundall's TRUBAL v. 1.51). Hongwei Yin would also like to thank Prof. Morgan and Rice University for hosting his collaborative visit in 2009, providing him with the opportunity to further develop his knowledge of DEM and geomechanics principles and to learn the capabilities of these methods. Many thanks to Prof. Huiqun Zhou, Prof. Chun Liu, and Dr. Qian Huang for their discussions on the development of VBOX. The relevant data and MATLAB and PFC codes used in this paper are available online: http://www.geovbox.com; more examples are given on the website. The authors are grateful to the anonymous reviewers for their many valuable suggestions that notably improved the manuscript.

Supplemental Data

The relevant MATLAB codes for the analytical solutions (main_Solve_T1_T2_T3_T4.m and Fs.m) and PFC codes for the numerical solutions (Fn_T1_T2final.txt, Fs_T3_T4final.txt, and fishcall.FIS) used in this paper are available online in the ASCE Library (www.ascelibrary.org).

References

Antonellini, M. A., and D. D. Pollard. 1995. "Distinct element modeling of deformation bands in sandstone." *J. Struct. Geol.*, 17(8), 1165–1182.

Asmar, B. N., P. A. Langston, A. J. Matchett, and J. K. Walters. 2002. "Validation tests on a distinct element model of vibrating cohesive particle systems." *Comput. Chem. Eng.*, 26(6), 785–802.

Balevičius, R., A. Džiugys, and R. Kačianauskas. 2004. "Discrete element method and its application to the analysis of penetration into granular media." *J. Civil Eng. Manage.*, 10(1), 3–14.

Botter, C., N. Cardozo, S. Hardy, I. Lecomte, and A. Escalona. 2014. "From mechanical modeling to seismic imaging of faults: A synthetic workflow to study the impact of faults on seismic." *Mar. Pet. Geol.*, 57, 187–207.

Botter, C., N. Cardozo, S. Hardy, I. Lecomte, G. Paton, and A. Escalona. 2016. "Seismic characterisation of fault damage in 3D using mechanical and seismic modelling." *Mar. Pet. Geol.*, 77, 973–990.

Burbidge, D. R., and J. Braun. 2002. "Numerical models of the evolution of accretionary wedges and fold-and-thrust belts using the distinct-element method." *Geophys. J. Int.*, 148(3), 542–561.

Chen, F., E. C. Drumm, and G. Guiochon. 2007. "Prediction/verification of particle motion in one dimension with the discrete-element method." *Int. J. Geomech.*, 344–352. 10.1061/(ASCE)1532-3641(2007)7:5(344).

Cundall, P. A., and O. D. L. Strack. 1979. "A discrete numerical model for granular assemblies." *Géotechnique*, 29(1), 47–65.

Damjanac, B., and P. Cundall. 2016. "Application of distinct element methods to simulation of hydraulic fracturing in naturally fractured reservoirs." *Comput. Geotech.*, 71, 283–294.

Finch, E., S. Hardy, and R. Gawthorpe. 2003. "Discrete element modelling of contractional fault-propagation folding above rigid basement fault blocks." *J. Struct. Geol.*, 25(4), 515–528.

Hardy, S., and E. Finch. 2006. "Discrete element modelling of the influence of cover strength on basement-involved fault-propagation folding." *Tectonophysics*, 415(1–4), 225–238.

Hardy, S., K. McClay, and J. A. Muñoz. 2009. "Deformation and fault activity in space and time in high-resolution numerical models of doubly vergent thrust wedges." *Mar. Pet. Geol.*, 26(2), 232–248.

Itasca. 2004. *PFC2D users' manual (version 3. 1).* Itasca Consulting Group, Inc., Minneapolis.

Iwashita, K., and M. Oda. 2000. "Micro-deformation mechanism of shear banding process based on modified distinct element method." *Powder Technol.*, 109(1–3), 192–205.

Kazerani, T., and J. Zhao. 2010. "Micromechanical parameters in bonded particle method for modelling of brittle material failure." *Int. J. Numer. Anal. Methods Geomech.*, 34(18), 1877–1895.

Liu, C., D. D. Pollard, K. Gu, and B. Shi. 2015. "Mechanism of formation of wiggly compaction bands in porous sandstone: 2. Numerical simulation using discrete element method." *J. Geophys. Res. B: Solid Earth*, 120(12), 8153–8168.

Liu, C., D. D. Pollard, and B. Shi. 2013. "Analytical solutions and numerical tests of elastic and failure behaviors of close-packed lattice for brittle rocks and crystals." *J. Geophys. Res. B: Solid Earth*, 118(1), 71–82.

Liu, C., Q. Xu, B. Shi, S. Deng, and H. Zhu. 2017. "Mechanical properties and energy conversion of 3D close-packed lattice model for brittle rocks." *Comput. Geosci.*, 103, 12–20.

Luding, S. 2008. "Cohesive, frictional powders: Contact models for tension." *Granular Matter*, 10, 235–246.

Matsu'ura, M., P. Mora, A. Donnellan, and X.-C. Yin. 2002. "Simulation of the micro-physics of rocks using LSMearth." *Earthquake processes: Physical modelling, numerical simulation and data analysis part I*, Birkha¨user Verlag, Basel, Switzerland, 1911–1932.

Mora, P., and D. Place 1993. "A lattice solid model for the nonlinear dynamics of earthquakes." *Int. J. Mod. Phys. C*, 4(6), 1059–1074.

Mora, P., and D. Place 1994. "Simulation of the frictional stick-slip instability." *Pure Appl. Geophys.*, 143(1–3), 61–87.

Mora, P., and D. Place 1998. "Numerical simulation of earthquake faults with gouge: Toward a comprehensive explanation for the heat flow paradox." *J. Geophys. Res. B: Solid Earth*, 103(B9), 21067–21089.

Mora, P., Y. Wang, and F. Alonso-Marroquin. 2015. "Lattice solid/Boltzmann microscopic model to simulate solid/fluid systems—A tool to study creation of fluid flow networks for viable deep geothermal energy." *J. Earth Sci.*, 26(1), 11–19.

Morgan, J. K. 1999. "Numerical simulations of granular shear zones using the distinct element method: 2. Effects of particle size distribution and interparticle friction on mechanical behavior." *J. Geophys. Res. B: Solid Earth*, 104(B2), 2721–2732.

Morgan, J. K. 2015. "Effects of cohesion on the structural and mechanical evolution of fold and thrust belts and contractional wedges: Discrete element simulations." *J. Geophys. Res. B: Solid Earth*, 120(5), 3870–3896.

Morgan, J. K., and M. S. Boettcher. 1999. "Numerical simulations of granular shear zones using the distinct element method: 1. Shear zone kinematics and the micromechanics of localization." *J. Geophys. Res. B: Solid Earth*, 104(B2), 2703–2719.

Place, D., and P. Mora. 1999. "The lattice solid model to simulate the physics of rocks and earthquakes: Incorporation of friction." *J. Comput. Phys.*, 150(2), 332–372.

Place, D., and P. Mora. 2001a. "A random lattice solid model for simulation of fault zone dynamics and fracture process." *Bifurcation and locatisation theory in Geomechanics*, H-B. Mühlhaus, A. V. Dyskin and E. Pasternak, eds., A.A. Balkema. Swets & Zeitlinger B.V., Lisse, 321–336.

Place, D., and P. Mora. 2001b. "Numerical simulation of localisation phenomena in a fault zone." *Microscopic and macroscopic simulation: Towards predictive modelling of the earthquake process*, Birkhäuser Verlag, Basel, Switerland, 1821–1845.

Saltzer, S. D., and D. D. Pollard. 1992. "Distinct element modeling of structures formed in sedimentary overburden by extensional reactivation of basement normal faults." *Tectonics*, 11(1), 165–174.

Schöpfer, M. P., C. Childs, T. Manzocchi, and J. J. Walsh. 2016. *Three-dimensional distinct element method modelling of the growth of normal faults in layered sequences.* Geological Society, London.

Shi, D., L. Zheng, J. Xue, and J. Sun. 2016. "DEM modeling of particle breakage in silica sands under one-dimensional compression." *Acta Mech. Solida Sin.*, 29(1), 78–94.

Smilauer, V., E. Catalano, B. Chareyre, S. Dorofeenko, J. Duriez, A. Gladky, J. Kozicki, C. Modenese, L. Scholtes, and L. Sibille. 2017. "Yade documentation." 2nd Ed. The Yade Project. ⟨https://www.yade-dem.org/doc/Yade.pdf⟩ (Feb. 9, 2018).

Yin, H., J. Zhang, L. Meng, Y. Liu, and S. Xu. 2009. "Discrete element modeling of the faulting in the sedimentary cover above an active salt diapir." *J. Struct. Geol.*, 31(9), 989–995.

Zhang, J., J. K. Morgan, G. G. Gray, N. W. Harkins, P. F. Sanz, and I. Chikichev. 2013. "Comparative FEM and DEM modeling of basement-involved thrust structures, with application to Sheep Mountain, Greybull area, Wyoming." *Tectonophysics*, 608, 408–417.